Nonstandard electroconvection in a bent-core nematic liquid crystal

D. Wiant and J. T. Gleeson
Department of Physics, Kent State University, Kent, Ohio 44242, USA

N. Éber and K. Fodor-Csorba
Research Institute for Solid State Physics and Optics, Hungarian Academy of Sciences, H-1525 Budapest, P.O. Box 49, Hungary

A. Jákli and T. Tóth-Katona
Liquid Crystal Institute, Kent State University, Kent, Ohio 44242, USA
(Received 11 April 2005; published 27 October 2005)

We characterize three nonstandard electrohydrodynamic instabilities in nematic liquid crystals composed of bent-core molecules. In addition to their shape, another important attribute of this material is that the anisotropy in the electrical conductivity changes sign as the frequency of the applied electric field changes. These instabilities do not appear to fit within the standard model for electroconvection. The first instability creates a pattern with stripes parallel to the initial director orientation, with a wavelength about equal to the separation of the cell plates. The next is the previously reported prewavy instability. The third instability is optically and dynamically identical to the prewavy instability, but is distinguished by different threshold behavior.

DOI: 10.1103/PhysRevE.72.041712 PACS number(s): 61.30.−v

I. INTRODUCTION

Nematic liquid crystals (NLC's), when driven out of equilibrium, can exhibit a rich variety of electroconvection (EC) patterns. These patterns result from the strong coupling between the NLC's orientational degrees of freedom, described by a unit vector field $\hat{n}$ (the director), the flow field, and the induced electric field. Because the anisotropies in the electrical transport properties (dielectric constant and conductivities) play such a critical role in EC, it is convenient to categorize NLC's according to the signs of these quantities. Specifically, the dielectric anisotropy ϵ_a is $\epsilon_\parallel - \epsilon_\perp$, where $\epsilon_\parallel$ is the dielectric permittivity for an electric field parallel to the director and $\epsilon_\perp$ is the component measured perpendicular to the director. Similarly the conductivity anisotropy σ_a describes the difference between the parallel and perpendicular components of the conductivity. There are four combinations of these anisotropies that can occur in a NLC, which can be written in the compact notation $(++)$, $(+-)$, $(-+)$, and $(--)$. Here the first sign represents the sign of the dielectric anisotropy and the second that of the conductivity anisotropy. For electro-optic information display purposes $(++)$ materials are by far the most commonly employed, while the vast majority of EC experimental and theoretical work has focussed on $(-+)$ materials. The Carr-Helfrich theory [1–4] predicts that EC will occur both in this latter case as well as in the unusual $(+-)$ situation.

For a system with an initial planar alignment, we choose a coordinate system such that the z axis runs perpendicular to the plates confining the liquid crystal, the x axis is parallel to the initial director orientation, and the y axis is perpendicular to the other two axes. (This coordinate system will be used in the remainder of this paper.) The Carr-Helfrich theory predicts, for the planar $(-+)$ case, spontaneous formation of a pattern of convective rolls perpendicular (or in some cases at an angle) to the x axis with a periodicity close to twice the spacing between the plates, d. This occurs as the applied potential difference is raised above a threshold voltage V_{th}. This is the scenario at low frequencies and is called the conductive regime. The theory also predicts that above a certain cutoff frequency f_c, there exists a pattern of shorter-wavelength stripes ($\lambda < d$), which also run perpendicular to the x axis. This is the dielectric regime. These patterns are formed due to a periodic modulation of the director in the xz plane, which can be explained by charge transport and convection effects. Both of these regimes have been extensively studied over the past few decades (see [5] and references therein).

Recently studies of the other situations $(+-)$ [6], $(++)$ [7], and $(--)$ [8–10] also have started to attract attention. Recent work on $(--)$ and $(++)$ NLC's in a planar orientation has shown EC not described by the Carr-Helfrich theory. Of particular interest to this paper is the $(--)$ situation. Here patterns of oblique rolls with wavelengths of the order of d, running roughly parallel to the x axis, have been observed [8,9]. The mechanism which drives this pattern formation is not yet understood. Additionally, certain NLC's exhibit the so-called prewavy instability. The prewavy (or wide domain) instabilities have been experimentally observed and theoretically discussed by several authors [11–22]. The prewavy pattern consists of a set of alternating dark and bright stripes, which are most easily viewed between crossed polarizers. The stripes run in the y direction, perpendicular to the initial director direction. The prewavy instability corresponds to a periodic modulation of the director in the xy plane, unlike that described by the Carr-Helfrich theory which predicts director modulation in the xz plane. The prewavy pattern can further be distinguished from the Carr-Helfrich-type behavior by its long wavelength, $\lambda \sim 4d-8d$. The forementioned characteristics of the prewavy instability have been clearly defined, but little is understood of the mechanism that produces this instability. The prewavy instability shares some common features with somewhat better understood models, such as the anisotropic inertia mode

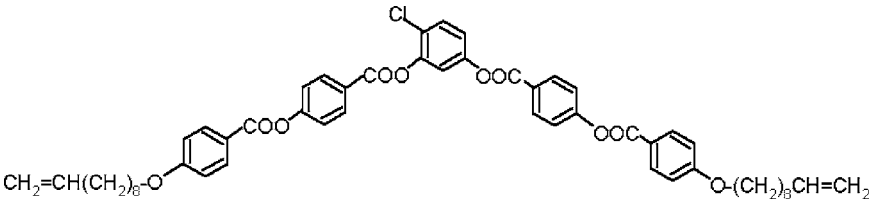

FIG. 1. Schematic chemical structure of 4-chloro-1,3-phenylene bis4 -[4′ - (9-decenyloxy)benzoyloxy] benzoate.

and the isotropic electrolyte mode, but ultimately differs from both these instabilities [18]. The prewavy instability is believed to be caused by an isotropic pattern formation mechanism, but further examination of this instability is needed to verify this conjecture.

Liquid crystals composed of bent-core, or banana-shaped, molecules have been the subject of a great deal of research in recent years due to their formation of ferroelectric phases [23–25], as well as the possibility of biaxial nematic phases [26–29]. The ways in which the bent molecules arrange and interact among themselves suggest a wealth of new phases [30] not seen in traditional LC's composed of rod-shaped molecules. Although many questions have been answered about banana-shaped LCs, there still is much that is not yet understood about these materials. As they become more prevalent in science and industry it is important to have a thorough understanding of banana-shaped LC's and their behavior under different conditions.

Few bent-core molecules exhibit a nematic phase [31–35], and up to now very little work has been done on EC in bent-core nematics (BCN). This paper will examine EC in the BCN labeled ClPbis10BB [36]. This compound shows three distinct frequency regions of EC instabilities, none of which seem to be explained by the Carr-Helfrich theory or a weakly nonlinear analysis, along with a region where no EC occurs.

In the remainder of this paper we will first discuss our experimental setup and methods. Then we will present and discuss the physical parameters of ClPbis10BB that are relevant for EC. Next, we will discuss each of the instabilities in order of their appearence with increasing frequency, beginning with the parallel stripe pattern observed at very low frequencies. This is followed by a wide stripe pattern, similar to the prewavy pattern, that is present between 30–1000 Hz. Then there is a region that does not show any EC up to about 5000 Hz. This is followed by another wide stripe pattern. We will examine the thresholds and characteristics of each region and attempt to begin to explain their formation mechanisms.

II. EXPERIMENT

The experiments were performed on the bent-core nematic liquid crystal 4-chloro-1,3-phenylene bis4-[4′-(9-decenyloxy)benzoyloxy]benzoate (ClPbis10BB) [36]. Its schematic chemical structure is shown in Fig. 1. ClPbis10BB exhibits a monotropic nematic phase upon cooling from 78 ± 1 °C to about 60 °C. This compound, with no added impurities, was placed in commercially obtained sandwich-type cells [37] with d of 10–50 μm. The surfaces of the cells were coated with transparent electrodes (indium tin oxide). The area of the conducting regions ranged from 100 mm^2 on the 10-μm cell to 50 mm^2 on the 50-μm cell. Cells for all EC and splay Freedericksz transition measurements were treated for planar alignment. All optical measurements were made using either a Zeiss Axiovert or a Nikon Optiphot polarizing microscope and a Panasonic charge-coupled-device (CCD) camera with a frame grabber. For these measurements the temperature was stabilized to ±0.1 °C using an Instec HS-1 hotstage. An ac voltage was sustained across the plates of the cell, which subjected the liquid crystal to an applied electric field $\vec{E}=(\sqrt{2}V/d)\cos(2\pi ft)\hat{z}$.

III. RESULTS AND DISCUSSION

A. Material properties

Because little is known about either a new material such as ClPbis10BB in particular or BCN's in general, we have measured some of the physical parameters important for EC. Specifically, the dielectric constants and conductivities, the splay and bend elastic constants, the anisotropy of the diamagnetic susceptibility (χ_a), and the rotational viscosity (γ_1) have been determined. The results of these experiments are presented in Table I.

Two sets of measurements of electrical transport properties were made by monitoring the capacitance C and conductance g of planar-aligned samples as they underwent the magnetic-field-induced Freedericksz transition [4]. The first, at a single-probe frequency of 1 kHz, employed an autobalancing Andeen Hagerling capacitance bridge to measure the capacitance and loss of a relatively thick sample ($d=55.1$ μm) as a function of magnetic field H. At this thickness we were able to reach approximately 6–7 times the Freedericksz threshold field H_F. At $H=0$ the perpendicular components $\epsilon_\perp$ and $\sigma_\perp$ could be measured directly. From

TABLE I. Material properties of ClPbis10BB.

$T_{NI}-T$ (°C)	$\epsilon_\perp$	$\epsilon_\parallel$	K_{11} (N)	K_{33} (N)
7.1	6.85	5.20	2.23×10^{-12}	2.37×10^{-12}
$\sigma_\perp$ (1/Ω m)	$\sigma_\parallel$ (1/Ω m)	χ_a (SI)	γ_1 (Pa s)	
1.58×10^{-7}	1.57×10^{-7}	1.76×10^{-7}	2.67	

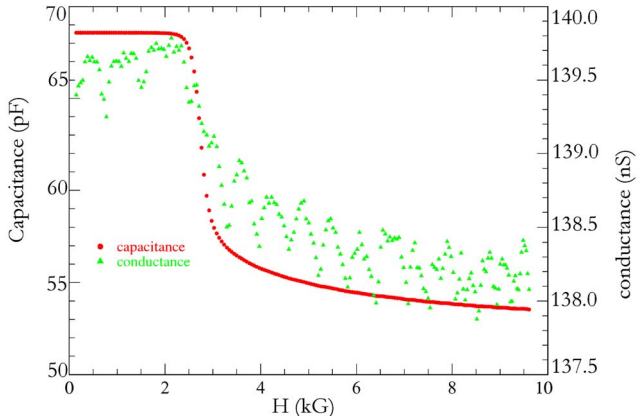

FIG. 2. (Color online) Example of the variation of the measured capacitance and conductance with magnetic field, at a temperature of 70 °C.

data at $H \gg H_F$ we could accurately extrapolate to infinite field and thus obtain the parallel components $\epsilon_\parallel$ and $\sigma_\parallel$. An example of such data is shown in Fig. 2. [The oscillations in the conductance plot in Fig. 2 are caused by temperature oscillations. The temperature was stable to about 6 mK in this experiment, which led to small (less than 0.4%) oscillationsin g. The only reason these are visible is because g only changes by around 1% over the the entire range of magnetic field.] The value of H_F gives us the ratio K_{11}/χ_a, while the slope of the $C(H)$ curve just above onset yields the ratio K_{33}/K_{11} [38].

The second measurement used a Quadtech 1920 frequency scanning *LCR* meter. For this measurement we used a thinner sample ($d=25$ μm), with which we could raise the magnetic field above H_F but could not accurately extrapolate data to infinite field. Therefore, these measurements—made at 70, 75, and 77 °C—only yielded the signs of ϵ_a and σ_a, but as functions of frequency. For the entire available frequency range (from 1 Hz to 100 kHz) at all three temperatures, with the magnetic field on ($H > H_F$) the capacitance was smaller than with the field off. Thus, $\epsilon_\perp > \epsilon_\parallel$—i.e., $\epsilon_a < 0$—for all temperatures and frequencies employed.

Conductance measurements revealed that σ_a has some unique features not usually seen in rodlike nematics. High-precision measurements on the $d=55.1$ μm sample at 1 kHz show the relative conductivity anisotropy $\sigma_a/\sigma_\perp$ to be less than 0.09 in magnitude and to become negative at about 3° below the clearing point T_{NI}. However, as the frequency is changed at a constant temperature the conductivity anisotropy changes sign twice, the sign being positive in an intermediate band between about 1.5 and 8 kHz for the $d=25$ μm sample. The location of the frequencies where the sign inversions of σ_a occur show a temperature dependence. Figure 3 demonstrates this behavior at 70 °C. The lower sign inversion frequency falls into the range 1500–1900 Hz; the upper sign inversion occurs between 8100 and 11 000 Hz. Upon increasing the temperature both sign inversion frequencies shift toward higher f. This is also exhibited in Fig. 8, below.

The double sign inversion of σ_a can be attributed to a dielectric relaxation process occurring in the specified frequency range. The dielectric loss has a frequency-dependent contribution to the conductivity, which has a maximum at the relaxation frequency f_r and decays when moving to either higher or lower f. The loss due to the relaxation in the parallel component can raise $\sigma_\parallel$ enough to induce the change from $\sigma_a < 0$ to $\sigma_a > 0$ and back near f_r. The relaxation in the parallel component should be accompanied by a reduction of $\epsilon_\parallel$. Indeed, the capacitance of the the cell with the magnetic field on showed a decrease as frequencies were increased, while no significant frequency dependence was found in the field off case (i.e., for $\epsilon_\perp$ and $\sigma_\perp$). Dielectric relaxation frequencies of nematics are generally in the MHz range (see

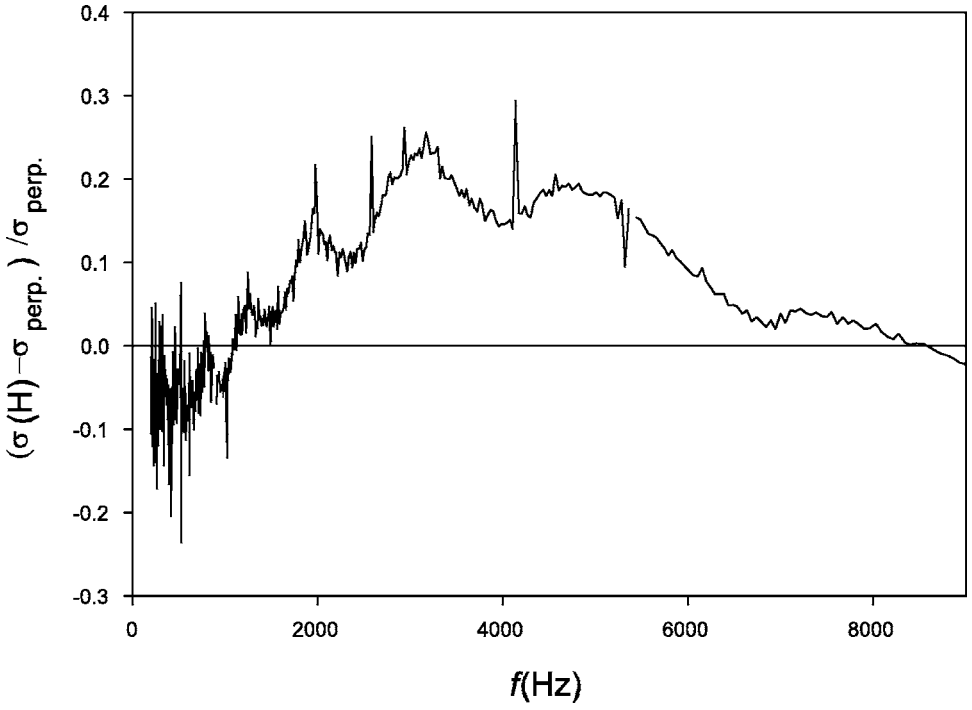

FIG. 3. This figure shows $[\sigma(H)-\sigma_\perp]/\sigma_\perp$, where $\sigma(H)$ is the (nearly) parallel component measured in the Freedericksz state with $H=10.9$ kG, which is well above the Freedericksz field, calculated to be 4.8 kG. σ_a is negative from 1 Hz to roughly 1500 Hz, positive for 1500→8100 Hz, and then negative again up to the end of the measurement at 100 kHz. These measurements were made on the 25-μm sample at 70 °C.

[39] and referneces therein). An f_r at about 4 kHz (as shown in Fig. 3) is quite unusual. The rare cases in which nematics is known to exhibit relaxation in the kHz range are, however, characterized by a (single) sign inversion of ϵ_a, and they show no change in the sign of σ_a; i.e., they exhibit a different behavior than the BCN tested.

By monitoring the rate of change of the capacitance as the magnetic field is raised above the critical field in a planar cell, we obtained the orientational relaxation time $\tau_1 = \gamma_1 d^2 / K_{11} \pi^2$, which yielded γ_1. We note that although backflow is expected in this geometry, its presence should not effect the time constant [40]. Finally, we measured the critical potential difference for the electric-field-induced bend Freedericksz transition by monitoring the light transmitted through a homeotropically aligned sample ($d=50$ μm) placed between crossed polarizers. This gives the ratio K_{33}/ϵ_a. Neither K_{11} nor K_{33} varies greatly with temperature, with K_{33} being larger than K_{11}. Thus, ClPbis10BB appears to possess similar elastic properties to rodlike calamitic liquid crystals (see [4] and references therein). However, $\chi_a = 1.76 \times 10^{-7}$ (in SI units) is about an order of magnitude smaller than that of calamitics (see [4] and references therein). Interestingly, however, γ_1 was found to range between 1.8 and 2.5 Pa s, which is more than 30 times larger than that of typical rodlike nematics such as methoxy benzylidene butylaniline (MBBA) [41] or pentylcyanobiphenyl (5CB) [42,43]. This clearly is a major contributor to the extreme slowness with which the various patterns respond to changes in the driving voltage and/or frequency.

B. Electroconvection

ClPbis10BB exhibits four very different scenarios at threshold as the frequency is changed. These four regimes are defined using Fig. 4, which shows threshold voltages V_{th} for the sample at 75 °C. All V_{th} values referred to were found by slowly raising the voltage and then waiting 15 min at the final voltage to see if a pattern became visible through crossed, or nearly crossed, polarizers. This process was then repeated with the voltage being lowered. The first region at 1–28 Hz, which we call the parallel stripe (PS) regime, has a linear frequency dependence of the threshold voltage as shown in the inset of Fig. 4. The next region is the prewavy2 (PW2) regime, from 28 to 1000 Hz. It is followed by the empty region (ER) at 1000–5000 Hz and finally by the prewavy1 (PW1) regime above 5000 Hz.

ClPbis10BB is $(--)$ in the PS region. The patterns observed here [Fig. 5(a)] are similar to those seen by Kochowska *et al.* [8] in $(--)$ calamitic liquid crystals. The PS pattern consists of stripes with wavelengths slightly less than d, which went from parallel to slightly oblique with regard to the initial director orientation. The best contrast was achieved when the polarizer and analyzer were a few degrees from perpendicular. This suggests that the director had periodic modulations in the xy plane. At 75 °C the pattern was visible from 1 to 24 Hz. Then at 25–27 Hz a coexistence of the parallel stripes and the perpendicular wide stripes (PW2, to be described below) could be seen [Fig. 5(b)]. At frequencies above 28 Hz, PS was no longer present. When the voltage was increased well above the threshold in PS a turbulent state could be observed [Fig. 5(d)].

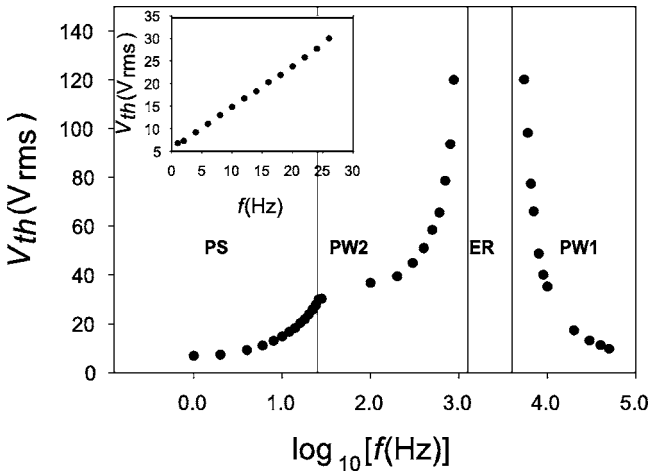

FIG. 4. Threshold curve for a 15-μm sample at 75 °C in the V-log(f) plane. Below 28 Hz parallel stripes (PS) are observed. From 28 to 1000 Hz a wide stripe pattern (PW2) is seen. The region from 1000 to 5000 Hz does not show any EC (ER). Above 5000 Hz another wide stripe pattern (PW1) is observed. Regions are separated by solid lines. The inset shows PS threshold versus frequency to better demonstrate the linearity of the threshold curve in this region.

V_{th} for PS is shown versus frequency at three different temperatures in Fig. 6(a). The frequency dependence of V_{th} remains linear while the temperature is changed. The slope of the threshold curve decreases as the temperature is increased. Figure 6(b) shows that V_{th} decreases monotonically as the clearing point is approached.

Flow patterns were not observed in the PS region. This is probably due to difficulties in detecting and measuring flow. The parallel stripes were narrow and tend to form in small, localized regions, which make it difficult to follow the flow of a dust particle.

Next we will discuss the ER. This region is unique because it appears to be void of any EC. The potential difference was increased up to 130 V_{rms}, which in this case produced an electric field of about 12.3 V/μm. This voltage was nearly large enough to cause dielectric breakdown, yet no EC was observed in this frequency range. Figure 7 shows the reciprocals of $V_{th}(f)$ in both the regions neighbouring the ER (PW1 at higher and PW2 at lower frequencies) for a sample at 75 °C. Each set of points could be well fitted with a straight line. Assuming that the linearity of $1/V_{th}(f)$ survives even at higher voltages, the lines were extrapolated to zero. The intersections enclose a band of frequency which suggests that the increase of the V_{th} on both sides of ER is not simply due to a divergence at a single frequency. Rather it points to an absence of EC at all voltages. Figure 8 shows that the PW1 region extends towards lower frequencies as the temperature is increased—i.e., the width of ER is reduced—but even within 0.5° of the clearing point the inverse of $V_{th}(f)$ still indicated an ER of finite width.

PW1 and PW2 are domains with wide stripes that run perpendicular to the x axis. The two modes are so named

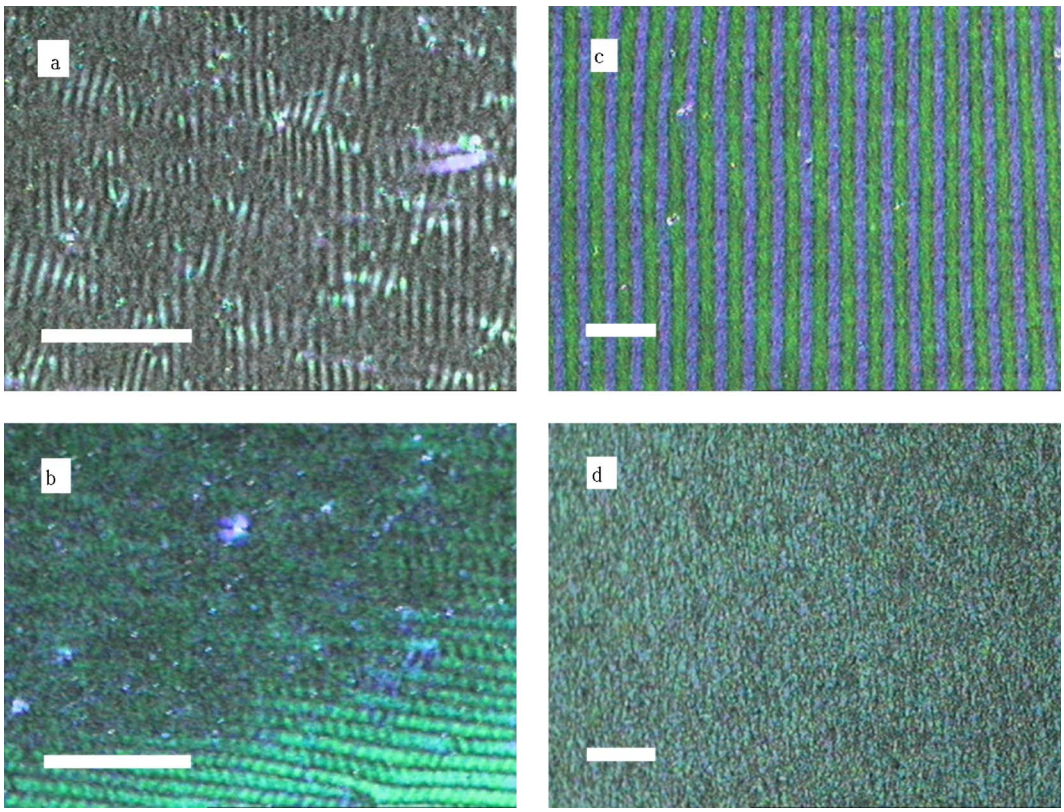

FIG. 5. (Color online) (a) PS at 12 Hz and 28 V_{rms}. (b) PS and PW2 coexisting at 26 Hz and 32 V_{rms}. (c) PW2 at 200 Hz and 48 V_{rms}. (d) Turbulent state at 5 Hz and 32 V_{rms}, which is well above threshold at this frequency. Images were taken with a 15-μm sample at 75 °C with crossed polarizers that were rotated $\sim 15°$ with respect to the vertical direction in the picture. Length scale represents 100 μm in each picture. In (a) and (b) the rubbing direction of the cell plates is in the vertical direction in the picture. In (c) and (d) the rubbing direction is in the horizontal direction in the picture.

because PW1 shows nearly identical characteristics to the prewavy mode described earlier [17,18], and PW2 shows many similarities to PW1. PW1 and PW2 are visually indistinguishable under a polarizing microscope, but are clearly separated in frequency by the ER and exhibit different threshold behaviors.

PW1 and PW2 show nearly identical optical and dynamic properties. The two patterns do seem to differ in a few regards though, which will be discussed before their similarities. First the shape of the $V_{th}(f)$ curve seems to show a stronger frequency dependence for PW2 than it does for PW1. Figure 9 shows that $V_{th}(T)$ for PW1 monotonically decreases as the clearing point is approached, while $V_{th}(T)$ for PW2 increases in the vicinity of T_{NI}.

Figure 8 shows that $V_{th}(f)$ for PW2 appears to diverge near the frequency were a change in the sign of the conductivity anisotropy occurs, without ever diverging at a frequency greater than the sign inversion frequency of σ_a. In contrast, $V_{th}(f)$ for PW1 appears not to be affected by the higher-frequency change in the sign of σ_a. The location of the higher sign inversion frequency of σ_a seems to show a stronger temperature dependence than that of the lower frequency one, just as $V_{th}(f)$ for PW1 shows a stronger temperature dependence than that of $V_{th}(f)$ for PW2.

Now, we will discuss the similarities of PW1 and PW2. Both regions form patterns on the order of hours, or days, versus the minutes it takes for the parallel stripes at low frequencies or for standard Carr-Helfrich patterns in other materials. Both patterns are only visible under crossed polarizers, indicating that director distortion remains in the xy plane. Both have stripes that are perpendicular to the initial director orientation and have $\lambda \sim 3d-4d$. Both patterns develop disclinations, which evolve into "wavy" patterns [44] at voltages much greater than the threshold (which were also viewed through crossed polarizers; see Fig. 10). All these optical properties are those of the previously described prewavy pattern.

The wavelength was measured at different points in the frequency-voltage plane in four different ways. The points could be reached quasistatically by holding one parameter fixed and varying the other slowly (with $dV/dt \sim 0.001$ V/s or $df/dt \sim 1$ Hz/s); rates of change increased to faster than about 0.005 V/s or 10 Hz/s would produce different patterns compared to the case when the parameters where changed more slowly. The pattern was allowed to relax for 1 h after the point was reached. A video camera and a frame grabber were then used to capture an image of the pattern. The camera was oriented so that the stripes were vertical in the captured image [as in Fig. 5(c)]. Then one color channel, red, green or blue, of the recorded image was selected. The color values (0–255) from each pixel in a vertical column were summed and divided by the number of pixels in the column to get the average instensity. This was repeated for

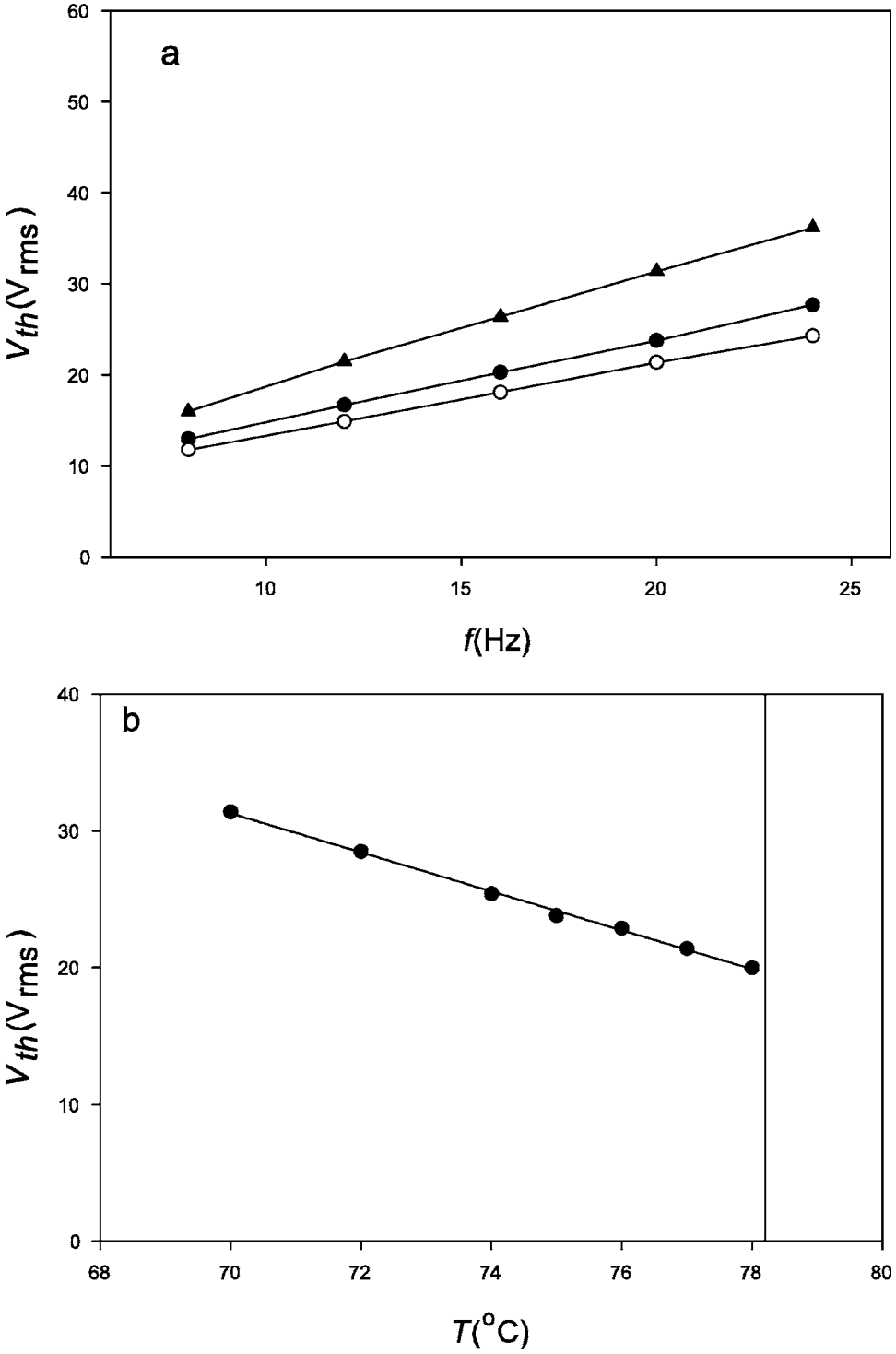

FIG. 6. (a) V_{th} versus frequency in the PS regime. Solid triangles, solid circles, and open circles represent data at 70, 75, and 77 °C, respectively. (b) Temperature dependence of V_{th} at 20 Hz in the PS regime. The clearing point is at 78.2 °C. Both measurements were made on a 15-μm sample.

every column in the image. This procedure provides an averaged intensity profile across the stripes. Next, the fast Fourier transform (FFT) of this profile was taken. The wavelength and its uncertainty could be obtained from the locations of the first four or five FFT peaks (for a complete description of this method see [45]). The choice of color channel used to calculate the averaged intensity profile had no effect on the results.

Slowly varying the voltage with f fixed or slowly varying the frequency with V fixed, to reach the same point in the V-f space, produced patterns with wavelengths that agreed with each other. In contrast, a different route to reach the same point in the V-f space was a rapid change of one of the parameters (going from an intial value to a final value in about 1 s), while the other was held fixed. Again, after 1 h the wavelength was measured as above. Quickly changing the voltage at constant f, or the frequency at constant V, again produced the same wavelengths. However, the final wavelength observed (described below) differed substan-

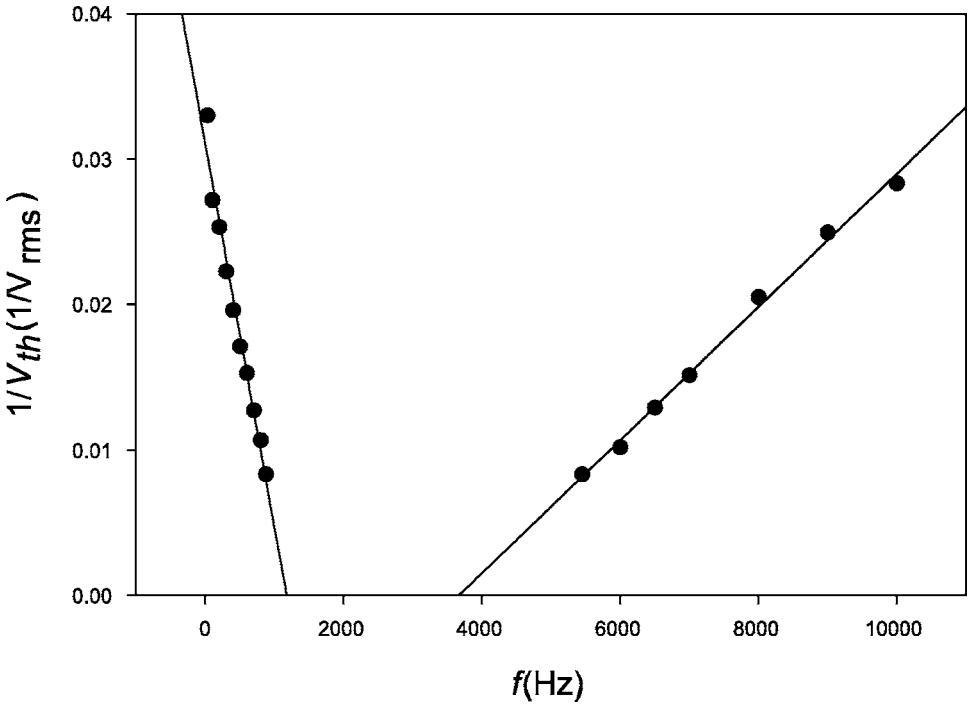

FIG. 7. The linear fits (solid lines) to $1/V_{th}(f)$ for PW2 (at low f) and PW1 (at high f) at 75 °C indicate that an ER exists even as $V_{th}(f) \to \infty$.

tially from that obtained using the previously described, quasistatic route.

Figure 11 shows that PW1 and PW2 exhibit similiar qualitative behavior in regards to how the wavelength varies with ε and f, where $\varepsilon = (V^2 - V_{th}^2)/V_{th}^2$. Quickly varying one parameter produced a pattern that contained many more dislocations, of both the types shown in Fig. 12, than a pattern produced by slowly varying a parameter. Quick variations produced a pattern with a shorter wavelength than did slow variations. Also, after a period of 48 h it was found that PW1 and PW2 patterns with dislocations, created by quickly varying the voltage, would relax to dislocation-free patterns with a slightly longer wavelength (than what was found after 1 h). Likewise, patterns formed by slowly varying the voltage would relax to a dislocation free pattern with a slightly shorter wavelength (than what was found after one hour); i.e., the wavelengths of the quickly varied and slowly varied patterns converge to an intermediate value after a certain time. This supports the idea that one stable, history-independent, pattern would be seen given enough time.

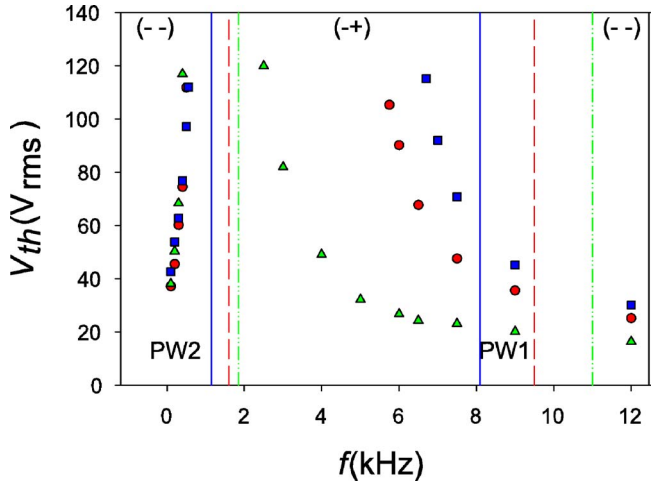

FIG. 8. (Color online) Frequency dependence of the threshold voltages for PW1 and PW2. Squares, circles, and triangles represent V_{th} at 70, 75, and 77 °C, respectively. The solid, dashed, and dash-dotted lines mark the frequencies where the sign of of σ_a changes at 70, 75, and 77 °C, respectively. These measurements were made on a 25-μm cell. $V_{th}(T)$ for PW1 shows a strong temperature dependence, while $V_{th}(T)$ for PW2 shows only a slight temperature dependence compared to PW1.

Another interesting pattern, which we will call the "knitting" instability (Fig. 13), was produced by abruptly raising the voltage from one of the prewavy states. After several hours the knitting instabilitity would relax to a stripe pattern with dislocations and would proceed to behave as the quickly varied state mentioned above. Several different types of long-wavelength instabilities have been observed in other materials during system relaxation from an initial state to a final state after a change of a control parameter—e.g., the Eckhaus, the zigzag, and the skewed varicose instabilities [46]. The knitting instability is believed to represent a new long-wavelength relaxation mechanism, which has not been previously observed.

All measurements from the previous sections were made with crossed polarizers. This configuration provides the best contrast for both PW1 and PW2. These patterns are also visible under nearly parallel polarizers with reduced contrast, but with one polarizer removed the pattern cannot be clearly optically discerned. The darker broad stripes in the prewavy patterns are produced by regions in which the director is roughly parallel, or perpendicular, to the polarizer. In this configuration the analyzer will block out the light. The brighter broad stripes are produced by regions where the director is at an angle to the polarizer. When the sample is rotated between crossed polarizers by 90° the directions parallel and perpendicular to the polarizer interchange but the

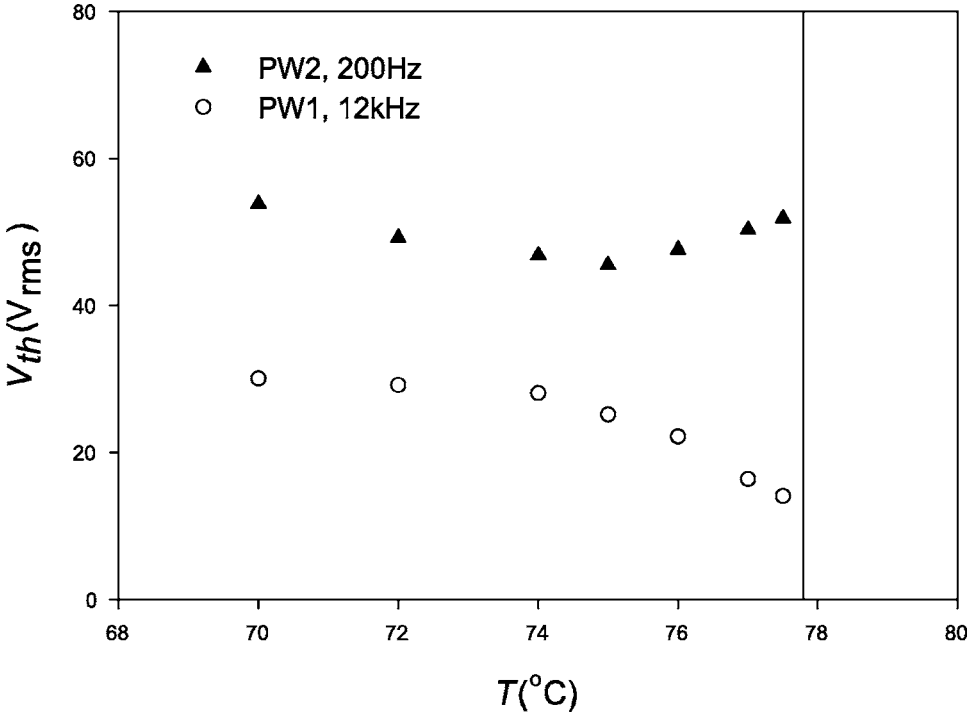

FIG. 9. Temperature dependence of threshold voltages for the prewavy regimes. Solid triangles represent $V_{th}(T)$ for PW2 at 200 Hz; open circles represent $V_{th}(T)$ for PW1 at 12 000 Hz. The clearing point is at 77.8 °C. Both measurements were made on a 25-μm sample.

intensities remain unchanged by this operation; thus, the optical appearance of the pattern has a 90° periodicity with respect to sample rotation. If the sample is rotated 45°, with respect to its initial position, the director for the darker stripes will be at an angle of 45° to the polarizer, which produces the greatest possible passage of light. As a result the darkest regions become the brightest, which means that the pattern is inverted from its initial state. The black lines between the broad stripes, most easily seen in Fig. 12, do not change color or intensity under rotation of the polarizers.

These observations reveal that the broad prewavy stripes are due to periodic director modulations in the xy plane [12,17] and that the director is in the $\hat{z}$ direction in the regions of the narrow black stripes. The voltage and frequency dependences of these director modulations were measured by rotating the sample under crossed polarizers. Initially, the sample was positioned so that the x axis was aligned with a polarizer. Then the sample was rotated in one direction until the optical intensity was minimized for the stripes that were initially bright—i.e., until the director of those stripes was aligned with the polarizer. This was then repeated with the sample being rotated in the opposite direction. The images obtained by rotations in opposite directions were inverted, which indicates that the director modulation is symmetric with respect to the initial director orientation ($\hat{x}$).

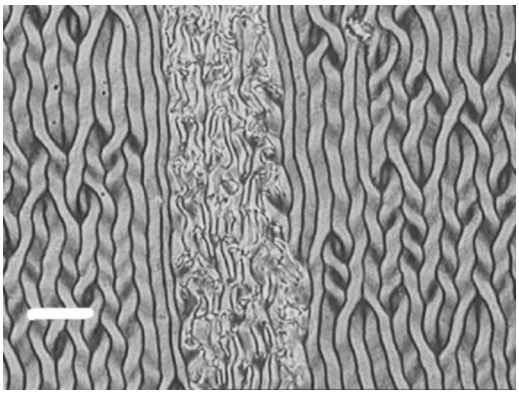

FIG. 10. Example of the wavy pattern, which is seen in the center region of the image, at 30 kHz and 55 V_{rms}. Image taken with a 10-μm sample at 70 °C between crossed polarizers that were rotated ~15° with respect to the vertical direction in the picture. The rubbing direction of the cell plates is in the horizontal direction of the picture; the length scale represents 100 μm.

The voltage dependence was measured at 100 Hz and 20 kHz by slowly varying the voltage and then recording the angle ϕ the director in the initially bright stripes made with respect to the x axis. This was then repeated with the voltage being quickly varied. (In both instances the voltage was changed in a manner similar to that described in the previous sections.) Similar measurements were made when varying the frequency at a fixed voltage. The amplitude of director modulations showed no frequency dependence in the observed region in either case.

Below the threshold voltage $\phi(V)=0$. For $V>V_{th}$, ϕ exhibits a supercritical pitchfork bifurcation. Figure 14 shows that $\phi(V)$ saturates at a value of about 23° for the slowly varied pattern and about 18° for the quickly varied pattern; in both cases, saturation occurs at voltages well above V_{th}. At 100 Hz (PW2), the director has a behavior similar to that of the 20-kHz (PW1) case [regarding the shape and the saturation values of the $\phi(V)$ curve], though over a different voltage range (40–50 V). Figure 14 also shows that the amplitude of the azimuthal director modulation obtained by slowly varying a parameter can be well fit by the formula

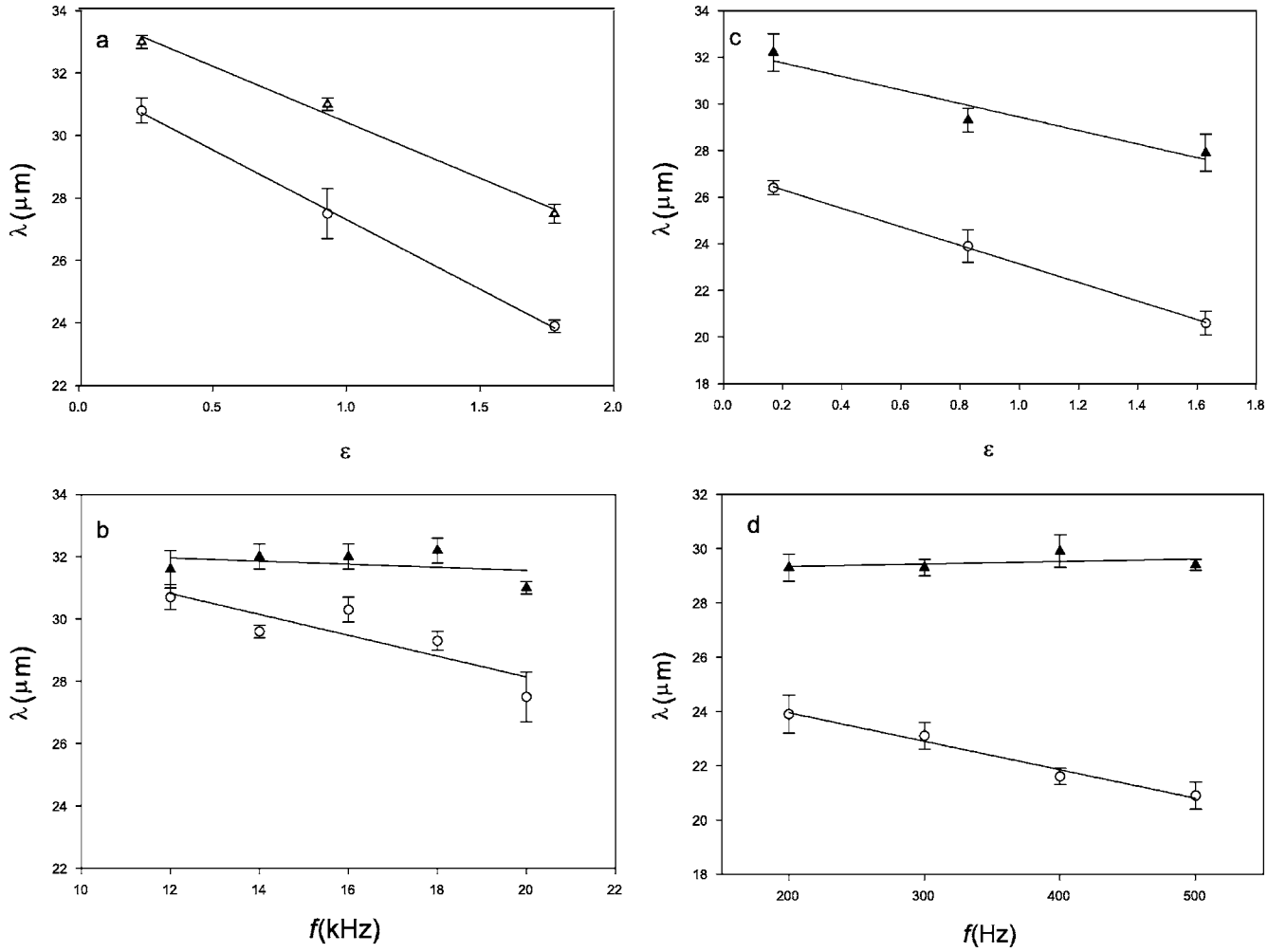

FIG. 11. (a) Wavelength as a function of ε at 20 kHz for PW1. (b) Wavelength as a function of frequency at 25 V_{rms} for PW1. (c) Wavelength as a function of ε at 200 Hz for PW2. (d) Wavelength as a function of frequency at 25 V_{rms} for PW2. In all charts the solid triangles and the open circles represent the pattern achieved by slowly varying and by quickly varying the voltage, respectively. All measurements were made on a 10-μm sample at 70 °C.

$$\phi(\varepsilon) = \phi_0 \sqrt{\frac{V^2 - V_{th}^2}{V_{th}^2}} \tag{1}$$

for voltages slightly above V_{th} [17].

The value of $\phi(\varepsilon)$ seems to be dependent on the way in which the point in the *V-f* space was reached, similar to the dependence shown for the wavelength. Also, the angular modulations of the states reached by quickly and slowly varying the voltage tend to converge to an intermediate value over time. This seems to show that a coupling between λ and ϕ can produce two quasistable history-dependent states, which exist for at least 24 h until the wavelengths and director modulations of the two states converge to form one stable state with intermediate λ and ϕ values.

The PW regimes had wider stripes and larger-scale patterns than the PS region; this made it possible to observe flow via dust particles. The flow was very slow, taking up to several hours to move across the field of view (about 500 μm) in some cases. Pictures were taken in 5-min intervals and then viewed to track the motion of the dust particles. The "zigzag" flow along the director (described in Ref. [18]) was the most frequently observed scenario. Dust particles were also observed to move in opposite directions, parallel to the stripes.

IV. CONCLUSION

In summary, we have observed and described three instabilities, along with a region in which no instabilities are observed, in bent-core nematic ClPbis10BB. The PS instability, observed at low frequencies, consists of a pattern of narrow stripes that run roughly parallel to the initial director orientation and have a linear threshold curve. The PW1 instability appears to represent an excellent example of the previously described prewavy instability, which is characterized by a wide stripe pattern and director modulation in the *xy* plane. The PW2 instability has nearly identical optical and dynamic properties to those of PW1, but the two instabilities show qualitatively different threshold behavior. The PW1 and PW2 regions are separated by the ER, where no EC was observed at fields higher than 12 V/μm. These observations leave

many questions unanswered, as the formation mechanisms for these regions are not yet understood.

The monotonic decrease of $V_{th}(T)$ as the clearing point is approached suggests that the threshold voltage of PS is not affected by the decrease in the conductivity and dielectric anisotropies in this region, which suggests that PS is driven by an isotropic mechanism, as opposed to an anisotropic mechanism. The threshold voltage of an instability driven by an anisotropic mechanism is expected to show a divergence near the clearing point because the voltage needed to drive the instability is expected to be inversely proportional to the anisotropy of the system (ϵ_a and σ_a), which becomes very small as T goes to T_{NI}.

However, there is also the possibility that the PS is caused by the flexoelectric effect. Nematic liquid crystals of bent-core (banana-shaped) molecules were first considered theoretically in 1969 by Meyer [47], who described a unique property of liquid crystals: flexoelectricity. In this effect a director deformation produces an electric polarization and alternatively an applied field induces a director deformation. Only splay and bend deformations result in macroscopic polarization with flexoelectric coupling constants e_1 and e_3, respectively. A molecular statistical approach for calculating the flexoelectric coefficients was subsequently developed by Helfrich [48]. This approach predicts in particular that the coefficient e_3 for banana-shaped molecules is proportional to the kink angle defined as $\beta=-180°-\psi$, where ψ is the opening angle between the molecular arms. For rod-shaped molecules $\psi\sim 180°$ and $\beta<1°$; however, for our banana-shaped molecule $\psi\sim 120°$—i.e., $\beta\sim 60°$. In conventional rod-shaped nematics, the flexoelectric coefficients are typically $10^{-11}-10^{-12}$ C/m; Helfrich's model suggests that BCN nematics may have coefficients 50 times greater than rodlike molecules. The flexoelectric effect has been reported to produce two kinds of patterns composed of parallel stripes with the wavelength on the order of d in calamitic liquid crystals—one at low frequencies [9,10,49–52] and another at high frequencies [9].

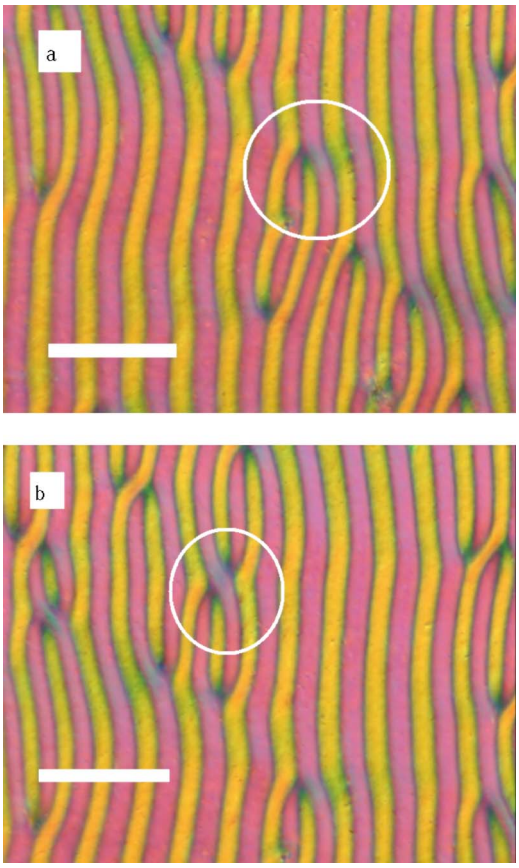

FIG. 12. (Color online) Examples of the two main types of dislocations which form in the prewavy regions. (a) The stripes appear to split apart. (b) The stripes appear to cross over or twist around each other. Both images taken at 20 kHz after quickly moving from 0 to 30 V_{rms} with a 10-μm sample at 70 °C between crossed polarizers that were rotated ~15° with respect to the vertical direction in the picture. The rubbing direction of the cell plates is in the horizontal direction in the pictures; the length scales represent 100 μm.

The high-frequency longitudinal rolls observed by Blinov *et al.* [9] were not related to flexoelectricity at the time of their discovery. It was proposed later in Ref. [52] that the reported pattern might be caused by the flexoelectric effect. This high-frequency flexoelectric pattern consists of randomly oriented longitudinal domains and was observed in a calamitic $(--)$ material. These domains had periods less than d, which were independent of temperature. V_{th} for these patterns showed a linear frequency dependence and was proportional to the cell thickness—i.e., had a field threshold. PS shares many of these traits. PS was oriented in small domains that went from parallel to oblique with λ slightly less than d. PS showed a weak temperature dependence and V_{th} for PS exhibited a linear frequency dependence.

It was proposed in Ref. [52] that the high-frequency flexoelectric regime in $(--)$ materials is analogous to the dielectric regime in $(-+)$ materials; i.e., it is an anisotropic mode. It was stated previously that the threshold voltage of an anisotropic mode generally shows a divergence as T_{NI} is

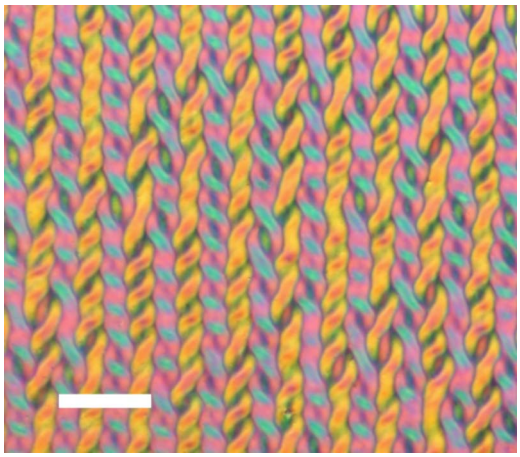

FIG. 13. (Color online) The "knitting" instability at 40 kHz and 35 V_{rms}. It is produced by abruptly raising the voltage from one of the prewavy states. Image taken with a 10-μm sample at 70 °C between crossed polarizers that were rotated ~15° with respect to the vertical direction in the picture. The rubbing direction of the cell plates is in the horizontal direction in the picture; the length scale represents 100 μm.

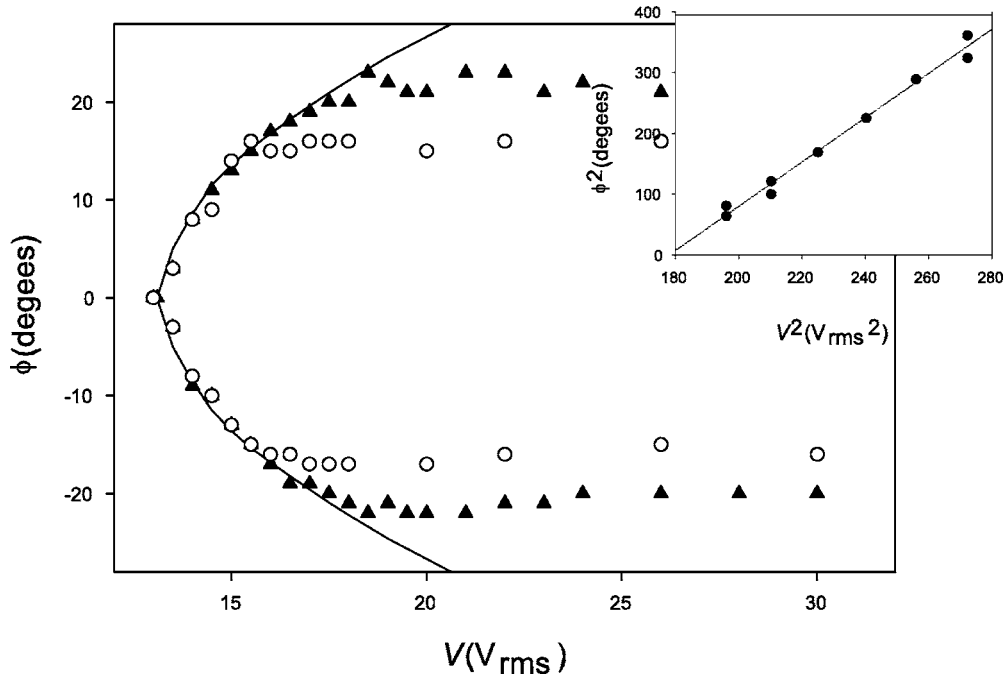

FIG. 14. Maxima of the azimuthal director modulation measured at 20 kHz and 70 °C. The solid triangles and the open circles show the director angle found by slowly varying and by quickly varying the voltage, respectively. The solid line shows the fit to Eq. (1) with $\phi_0 = 22.4°$ for the case where the voltage was slowly varied. The inset shows that the goodness of the fit can be better demonstrated by manipulating Eq. (1) to the form $\phi^2 = (\phi_0/V_{th})^2 V^2 - \phi_0^2$, which more clearly shows the linear relation between ϕ^2 and V^2. Again, this was done for the case where the voltage was slowly varied. The fact that the ϕ values saturated at higher voltages made it difficult to discern the point where the quadratic behavior ended, so there is an amount of uncertainty introduced into the fit of the straight line depending on how many data points are used.

approached. However, this is not always the case. Certain materials that exhibit Carr-Helfrich-type instabilities, such as phase 5 (Merck), do not show a divergence in V_{th} at the clearing point. This apparent discrepancy is believed to be related to the nature of the N-I transition. A divergence is in fact only expected for weakly first-order transitions, where the anisotropies go to zero almost continuously. If the anisotropies show only a weak temperature dependence and then fall to zero suddenly at T_{NI}, a divergence might not be present. The substance ClPbis10BB exhibits a fairly large jump of ϵ_a near T_{NI} at 1 kHz. Thus a lack of divergence of V_{th} near T_{NI} would not be surprising. It means that one cannot exclude the possibility that PS is driven by an anisotropic mechanism, like the high-frequency flexoelectric mode mentioned above. If this were the case, PS might still be explained by the standard model after incorporating the flexoelectric effect.

Let us now focus on the prewavy modes PW1 and PW2. It was shown in the previous section that the characteristics of the PW1 instability correspond to those of the prewavy pattern [18], except for the frequency dependence of the thresholds. The optical appearance and the dynamical behavior of PW2 was found to be almost identical to those of PW1. One interpretation of the situation, based on the differences in the temperature and frequency dependences of the threshold voltages, is that PW1 and PW2 are of different origins. PW2 exhibits a divergent $V_{th}(f)$ at a frequency near the sign inversion frequency of σ_a, without ever being greater than the sign inversion frequency. Also, PW2 always has an increase in $V_{th}(T)$ as the clearing point is approached. These features are strong evidence that PW2 may be caused by an anisotropic mechanism. On the contrary, PW1 seems to be unrelated to the sign inversion of σ_a and shows a monotonic decrease of $V_{th}(T)$ through the clearing point. These observations seem to indicate that PW1 is caused by an isotropic mechanism. In the ER, which separates the two prewavy modes in frequency, the BCN studied is $(-+)$, so a Carr-Helfrich-type instability could be expected, yet is not observed. There is no explanation as to why no EC exists in this region.

Unfortunately no rigorous theoretical treatment of the isotropic electroconvection modes has been developed at this time which could give an account of the mechanism of the prewavy pattern. Nor has the influence of a frequency-dependent ϵ_a and σ_a been fully analyzed within the framework of the standard model, which could answer how the observed dielectric relaxation is related to the current situation. The few reports of electroconvection associated with dielectric relaxation [39,53] concern substances applicable for dual frequency addressing—i.e., exhibiting a sign inversion of ϵ_a at increasing f, but having $\sigma_a > 0$ at all frequencies—which are not relevant to our case.

ACKNOWLEDGMENTS

We have benefited from fruitful discussions with A. Buka and technical assistance from G. Liao. This work was supported by the NSF (Grant Nos. DMR-9988164 and OISE-

0225963) and the U.S. Department of Education as well as the NSF-MTA-OTKA joint Project No. 78 and the Hungarian Research Funds OTKA-T037336, OTKA-T032667, and NKFP-128/6.

[1] E. F. Carr, Mol. Cryst. Liq. Cryst. **7**, 253 (1969).
[2] W. Helfrich, J. Chem. Phys. **51**, 4062 (1969).
[3] L. M. Blinov and V. G. Chigrinov, *Electrooptic Effects in Liquid Crystal Materials* (Springer-Verlag, Berlin, 1994).
[4] P. G. de Gennes and J. Prost, *The Physics of Liquid Crystals* (Oxford Science, Oxford, 1993).
[5] A. Buka and L. Kramer, *Pattern Formation in Liquid Crystals* (Springer-Verlag, Berlin, 1996).
[6] A. Buka, B. Dressel, W. Otowski, K. Camara, T. Toth-Katona, L. Kramer, J. Lindau, G. Pelzl, and W. Pesch, Phys. Rev. E **66**, 051713 (2002).
[7] B. Dressel and W. Pesch, Phys. Rev. E **67**, 031707 (2003).
[8] E. Kochowska, S. Nemeth, G. Pelzl, and A. Buka, Phys. Rev. E **70**, 011711 (2004); El. Liq. Cryst. Commun., ⟨http://www.e-lc. org/docs/2004_01_23_11_12_27⟩.
[9] L. M. Blinov, M. I. Barnik, V. T. Lazareva, and A. N. Trufanov, J. Phys. (Paris), Colloq. **40**, C3-263 (1979).
[10] M. Goscianski and L. Leger, J. Phys. (Paris), Colloq. **36**, C1-231 (1975).
[11] P. Petrescu and M. Giurgea, Phys. Lett. **59A**, 41 (1976).
[12] L. Nasta, A. Lupu, and M. Giurgea, Mol. Cryst. Liq. Cryst. **71**, 65 (1981).
[13] A. N. Trufanov, M. I. Barnik, and L. M. Blinov, Sov. Phys. JETP **51**, 314 (1980).
[14] S. Kai and K. Hirakawa, Solid State Commun. **18**, 1573 (1976).
[15] R. Ribotta and G. Durand, J. Phys. (Paris), Colloq. **40**, C3-334 (1979).
[16] W. Weissflog, G. Pelzl, H. Kresse, and D. Demus, Cryst. Res. Technol. **23**, 1259 (1988).
[17] J.-H. Huh, Y. Yusuf, Y. Hidaka, N. Eber, T. Toth-Katona, A. Buka, and S. Kai, Mol. Cryst. Liq. Cryst. Sci. Technol., Sect. A **364**, 111 (2001).
[18] J.-H. Huh, Y. Yusuf, Y. Hidaka, and S. Kai, Phys. Rev. E **66**, 031705 (2002).
[19] S. Komineas, H. Zhao, and L. Kramer, Phys. Rev. E **67**, 031701 (2003).
[20] M. I. Barnik, L. M. Blinov, S. A. Pikin, and A. N. Trufanov, Sov. Phys. JETP **45**, 396 (1977).
[21] S. A. Pikin and V. G. Chigrinov, Sov. Phys. JETP **51**, 123 (1980).
[22] W. Weissflog, S. Sokolowski, H. Dehne, B. Das, S. Grande, M. Schroder, A. Eremin, S. Diele, G. Pelzl, and H. Kresse, Liq. Cryst. **31**, 923 (2004).
[23] T. Niori, F. Sekine, J. Watanabe, T. Furukawa, and H. Takezoe, J. Mater. Chem. **6**, 1231 (1996).
[24] T. Sekine, T. Niori, M. Sone, J. Watanabe, S. W. Choi, Y. Takanishi, and H. Takezoe, Jpn. J. Appl. Phys., Part 1 **36**, 6455 (1997).
[25] D. R. Link, G. Natale, R. Shao, J. E. Maclennan, N. A. Clark, E. Korblova, and D. M. Walba, Science **278**, 1924 (1997).
[26] J. A. Oliveras, S. Stojadinovic, T. J. Dingemans, S. Sprunt, and A. Jakli, Phys. Rev. E **68**, 041704 (2003).
[27] B. R. Acharya, A. Primak, T. J. Dingemans, E. T. Samulski, and S. Kumar, Pramana, J. Phys. **61**, 231 (2003).
[28] L. A. Madsen, T. J. Dingemans, M. Nakata, and E. T. Samulski, Phys. Rev. Lett. **92**, 145505 (2004).
[29] B. R. Acharya, A. Primak, and S. Kumar, Phys. Rev. Lett. **92**, 145506 (2004).
[30] T. C. Lubensky and L. Radzihovsky, Phys. Rev. E **66**, 031704 (2002).
[31] J. Matraszek, J. Mieczkowski, J. Szydlowska, and E. Gorecka, Liq. Cryst. **27**, 429 (2000).
[32] I. Wirth, S. Diele, A. Eremin, G. Pelzl, S. Grande, L. Kovalenko, N. Pancenko, and W. Weissflog, J. Mater. Chem. **11**, 1642 (2001).
[33] W. Weissflog, H. Nadasi, U. Dunemann, G. Pelzl, S. Diele, A. Eremin, and H. Kresse, J. Mater. Chem. **11**, 2748 (2001).
[34] E. Matyus and K. Keseru, J. Mol. Struct. **543**, 89 (2001).
[35] T. J. Dingemans and E. T. Samulski, Liq. Cryst. **27**, 131 (2000).
[36] K. Fodor-Csorba, A. Vajda, G. Galli, A. Jakli, D. Demus, S. Holly, and E. Gacs-Baitz, Macromol. Chem. Phys. **203**, 1556 (2002).
[37] E.H.C. Co., Tokyo, Japan.
[38] Hp. Schad, B. Scheuble, and J. Nehring, J. Chem. Phys. **71**, 5140 (1979).
[39] W. H. De Jeu, C. J. Gerritsma, and W. J. A. Goosens, Phys. Lett. **39A**, 355 (1972).
[40] F. Brochard, Mol. Cryst. Liq. Cryst. **23**, 51 (1973).
[41] H. Kneppe, F. Schneider, and N. K. Sharma, J. Chem. Phys. **77**, 3203 (1982).
[42] K. Skarp, S. T. Lagerwall, and B. Stebler, Mol. Cryst. Liq. Cryst. **60**, 215 (1980).
[43] M. Cui and J. R. Kelly, Mol. Cryst. Liq. Cryst. Sci. Technol., Sect. A **331**, 1909 (1999).
[44] J.-H. Huh, Y. Hidaka, A. G. Rossberg, and S. Kai, Phys. Rev. E **61**, 2769 (2000).
[45] J. T. Gleeson, Phys. Rev. E **54**, 6424 (1996).
[46] S. Kai, Y. Adachi, and S. Nasuno, in *Spatio-Temporal Patterns*, edited by P. Cladis and Palffy-Muhoray (Addison-Wesley, Reading, MA, 1995).
[47] R. B. Meyer, Phys. Rev. Lett. **22**, 918 (1969).
[48] W. Helfrich, Z. Naturforsch. A **26**, 833 (1971).
[49] M. I. Barnik, L. M. Blinov, B. A. Umansky, and A. N. Trufanov, J. Phys. (Paris) **39**, 417 (1978).
[50] L. M. Blinov, J. Phys. (Paris), Colloq. **40**, C3-247 (1979).
[51] Y. Bobylev, V. G. Chigrinov, and S. Pikin, J. Phys. (Paris), Colloq. **40**, C3-331 (1979).
[52] N. V. Madhusudana and V. A. Raghunathan, Liq. Cryst. **5**, 1789 (1989).
[53] V. G. Chigrinov, A. Sparavigna, and A. Strigazzi, Phys. Rev. E **53**, 4918 (1996).